Results in Physics 44 (2023) 106175

Contents lists available at ScienceDirect

Results in Physics

journal homepage: www.elsevier.com/locate/rinp

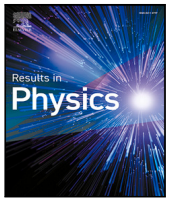

Comparative analysis of numerical with optical soliton solutions of stochastic Gross–Pitaevskii equation in dispersive media

Muhammad Zafarullah Baber [a], Nauman Ahmed [a], Muhammad Waqas Yasin [a,c], Muhammad Sajid Iqbal [b], Ali Akgül [d,e,i], Muhammad Bilal Riaz [f,*], Muhammad Rafiq [g,i], Ali Raza [h]

[a] Department of Mathematics and Statistics, The University of Lahore, Lahore, Pakistan
[b] Department of Humanities & Basic Science, Military College of Signals, NUST, Islamabad, Pakistan
[c] Department of Mathematics, University of Narowal, Narowal, Pakistan
[d] Department of Computer Science and Mathematics, Lebanese American University, Beirut, Lebanon
[e] Siirt University, Art and Science Faculty, Department of Mathematics, 56100 Siirt, Turkey
[f] Faculty of Applied Physics and Mathematics, Gdańsk University of Technology, Narutowicza 11/12, 80-233 Gdańsk, Poland
[g] Department of Mathematics, Faculty of Sciences and Technology, University of Central Punjab, Lahore, Pakistan
[h] Department of Mathematics, Govt. Maulana Zafar Ali Khan Graduate College Wazirabad, 52000, Punjab Higher Education Department (PHED), Lahore, 54000, Pakistan
[i] Near East University, Mathematics Research Center, Department of Mathematics, Near East Boulevard, PC: 99138, Nicosia/Mersin 10, Turkey

ARTICLE INFO

Keywords:
Proposed SNSFD scheme
Stability analysis of scheme
Consistency of scheme
Exact solutions
Stochastic Gross–Pitaevskii equation (SGPE)
SSE technique
MERF technique

ABSTRACT

This article deals with the stochastic Gross–Pitaevskii equation (SGPE) perturbed with multiplicative time noise. The numerical solutions of the governing model are carried out with the proposed stochastic non-standard finite difference (SNSFD) scheme. The stability of the scheme is proved by using the Von-Neumann criteria and the consistency is shown in the mean square sense. To seek exact solutions, we applied the Sardar subequation (SSE) and modified exponential rational functional (MERF) techniques. The exact solutions are constructed in the form of exponential, hyperbolic, and trigonometric forms. Finally, the comparison of the exact solutions with numerical solutions is drawn in the 3D and line plots for the different values of parameters.

Introduction

In this modern era of research, seeking the exact solutions of nonlinear partial differential equations (NLPDEs) is a very important topic, because NLPDEs have physical complex phenomena in different fields such as physics, biology, mechanics, biomathematics, mechanics, etc. [1–4]. The Gross–Pitaevskii equation (GPE) is a classical nonlinear evolution [5]. It is the type of famous nonlinear Schrödinger equation. The NLSE is a universal governing model that evolution of complex fields that are used in dispersive media [6,7]. A Bose–Einstein condensate (BEC) made up of N can be modeled using the GPE, which is a classical field equation with applications to the propagation of light in optical fibre, planar waveguides, and Bose–Einstein condensates constrained to highly anisotropic sigar-shaped traps in the mean-field regime of dilute gases, as noted in [8–10]. This equation can also be found in the research of Langmuir waves in hot plasmas, small wave-amplitude gravity waves on the surface of deep inviscid (zero-viscosity) water, plane-diffracted wave beams in the focusing regions of the ionosphere, Davydov's alpha-helix solitons, which are responsible for energy transfer along molecular chains, and many other phenomena.

At the micro level, every mathematical model physically does not appear in the linear motion but has a random motion. So, for the sake of randomness, many researchers use the multiplicative white noise in the mathematical model [11]. By appearing this term differential equations called the stochastic differential equation.

When we see most of the physical phenomena at the micro-scale and magnify them, then these phenomena are stochastic or random phenomena. It is very natural to consider the differential equation which has some kind of randomness involved. So, if this randomness is going bounded in the solution of the differential equations, such problems are stochastic differential equations. The numerical solutions of the stochastic NLPDEs are estimated by some scientists [12,13]. They developed the numerical schemes and the simulations and also gives the stability and consistency of schemes [14]. The "Good" Boussinesq equation have been studied numerically by using different techniques [15–17]. For more literature on SPDE's [18–27]. In this current era of research many researchers are working on the different stochastic NLPDEs, numerically and analytically but their is a gape

* Corresponding author.
E-mail address: bilalsehole@gmail.com (M.B. Riaz).

https://doi.org/10.1016/j.rinp.2022.106175
Received 23 October 2022; Received in revised form 6 December 2022; Accepted 10 December 2022
Available online 17 December 2022

of the comparison of the results. So, in this study we compare the numerical result with exact solitary wave solutions by simulations. For the simulations of result we use the MATLAB 2015a. For the sake of exact solutions, many researchers also use multiplicative white noise and show the randomness in their solutions [28,29]. But in this study, we use the both numerical and analytical solutions to compare the graphical simulations with the noise effect. The aim of finding the exact solutions vast variety of powerful and direct methods are used named as, He's variational iteration [30–33], new modified extended direct algebraic [34,35], G'/G-expansion [36,37], ϕ^6-model expansion [38, 39], hirota bilinear [40,41], modified exponential rational functional method [42,43], etc. The numerical approximation of the some partial differential equations are carried out such as [44–50].

The comparison of numerical solutions of the stochastic differential equation with analytical or solitary wave solutions is not a simple job, it becomes more difficult when our governing equation is a nonlinear stochastic differential equation and we have tried to overcome such issues. But in this study, the underlying SGPE model is investigated numerically and analytically. But the main purpose of this study is the comparison of exact and numerical solutions under the effect of time noise.

The main contribution and novelty of the current study is as follow:

- The Gross–Pitaevskii equation under the influence of the time noise is under consideration.
- The numerical solutions are derived by proposed stochastic NSFD scheme.
- The analysis of the scheme is proved in mean square sense.
- The solitary wave solutions are extracted by two techniques namely Sardar subequation (SSE) and modified exponential rational (MERF).
- The comparison of some solitary wave solutions with numerical solutions are represented by simulations.

Governing model

The stochastic Gross–Pitaevskii equation (SGPE) suitable units, in one-dimension can be taken as [1–8],

$$i\Phi_t = -\frac{1}{2}\Phi_{xx} + V(x)\Phi + g|\Phi|^2\Phi + \sigma\dot{W}(t)\Phi, \tag{1}$$

where $\Phi(x,t)$ represents the macroscopic wave function of the condensate, $V(x)$ is a real-valued function that generated macroscopic potential experimentally. The parameter g encapsulates the strength of the atom–atom interactions. Which determine whether this model is repulsive when the value of g is 1 (defocusing nonlinearity) or shows attraction when g is -1, (focusing nonlinearity) [51]. Here, σ is represents the strength of the Brownian motion and $\dot{W}(t)$ is the random function.

Proposed stochastic non-standard finite difference (NSFD) scheme

The Φ_t and Φ_{xx} in Eq. (12) are approximated as follows,

$$\Phi_t = \frac{\Phi_p^{q+1} - \Phi_p^q}{k}, \qquad \Phi_{xx} = \frac{\Phi_{p+1}^q - 2\Phi_p^{q+1} + \Phi_{p-1}^q}{h^2},$$

here, space and time stepsizes are take as $h = \Delta x^2$ and $k = \Delta t$ respectively. The state variable Φ_p^q is the approximation of $\Phi(x,t)$ at $\Phi(p\Delta x, q\Delta t)$. Now,by replacing the values of Φ_t and Φ_{xx} in Eq. (12) and after some basic arithmetics, we get

$$\begin{aligned}(i+2\alpha)\Phi_p^{q+1} &= \alpha\Phi_{p+1}^q + \alpha\Phi_{p-1}^q + (i+kV_p)\Phi_p^q + gk|\Phi_p^q|^2\Phi_p^q \\ &\quad + k\sigma\Phi_p^q(W^{(q+1)k} - W^{qk}),\end{aligned} \tag{2}$$

where $\alpha = \frac{-k}{2h^2}$. The Eq. (2) is required proposed finite difference scheme for Eq. (12).

Consistency of scheme

The consistency of the scheme is proved in the mean square sense [13,14].

Theorem 1. *The proposed stochastic NSFD scheme for Φ in (2) is consistent with (12), in mean square sense.*

Proof. We suppose the smooth function $\Phi(x,t)$ and using the operator $Z(\Phi) = \int_{q\Delta t}^{(q+1)\Delta t}(\Phi)ds$. Apply this on Eq. (12) and get as follows;

$$\begin{aligned}Z(\Phi)_p^q &= \Phi(p\Delta x,(q+1)\Delta t) - \Phi(p\Delta x,q\Delta t) + \frac{d}{2}\int_{q\Delta t}^{(q+1)\Delta t}\Phi_{xx}(p\Delta x,s)ds \\ &\quad -V(x)\int_{q\Delta t}^{(q+1)\Delta t}\Phi(p\Delta x,s)ds \\ &\quad -g\int_{q\Delta t}^{(q+1)\Delta t}|\Phi(p\Delta x,s)|^2\Phi(p\Delta x,s)ds \\ &\quad -\sigma\int_{q\Delta t}^{(q+1)\Delta t}\Phi(p\Delta x,s)dW|_s,\end{aligned} \tag{3}$$

$$\begin{aligned}Z|_p^q(\Phi) &= \Phi(p\Delta x,(q+1)\Delta t) - \Phi(p\Delta x,q\Delta t) \\ &\quad + \frac{d}{2}\Delta t\frac{\Phi((p+1)\Delta x,q\Delta t) - 2\Phi(p\Delta x,(q+1)\Delta t) + \Phi((p-1)\Delta x,q\Delta t)}{\Delta x^2} \\ &\quad -V(x)\Delta t\Phi(p\Delta x,q\Delta t) - g\Delta t|\Phi(p\Delta x,q\Delta t)|^2\Phi(p\Delta x,q\Delta t) \\ &\quad -\sigma\Phi(p\Delta x,q\Delta t)(W^{(q+1)\Delta t} - W^{q\Delta t}),\end{aligned} \tag{4}$$

in the mean square sense the above relations take form as follows;

$$\begin{aligned}&E|Z(\Phi)_p^q - Z|_p^q(\Phi)|^2 \le d^2E|\int_{q\Delta t}^{(q+1)\Delta t}(\Phi_{xx}(p\Delta x,s) \\ &-\frac{\Phi((p+1)\Delta x,q\Delta t) - 2\Phi(p\Delta x,(q+1)\Delta t) + \Phi((p-1)\Delta x,q\Delta t)}{\Delta x^2})ds|^2 \\ &+4(V(x))^2E\left|\int_{q\Delta t}^{(q+1)\Delta t}(-\Phi(p\Delta x,s) + \Phi(p\Delta x,q\Delta t))ds\right|^2 \\ &+4g^2E\left|\int_{q\Delta t}^{(q+1)\Delta t}(-|\Phi(p\Delta x,s)|^2\Phi(p\Delta x,s)\right. \\ &\left.+|\Phi(p\Delta x,q\Delta t)|^2\Phi(p\Delta x,q\Delta t))ds\right|^2 \\ &+4\sigma^2E\left|\int_{q\Delta t}^{(q+1)\Delta t}(-\Phi(p\Delta x,s) + \Phi(q\Delta x,p\Delta t))\,dW|_s\right|^2,\end{aligned}$$

square property of the Itô's integral gives us,

$$\begin{aligned}&E|Z(\Phi)_p^q - Z|_p^q(\Phi)|^2 \le d^2E|\int_{q\Delta t}^{(q+1)\Delta t}(\Phi_{xx}(p\Delta x,s) \\ &-\frac{\Phi((p+1)\Delta x,q\Delta t) - 2\Phi(p\Delta x,(q+1)\Delta t) + \Phi((p-1)\Delta x,q\Delta t)}{\Delta x^2})ds|^2 \\ &+4(V(x))^2E\left|\int_{q\Delta t}^{(q+1)\Delta t}(-\Phi(p\Delta x,s) + \Phi(p\Delta x,q\Delta t))ds\right|^2 \\ &+4g^2E\left|\int_{q\Delta t}^{(q+1)\Delta t}(-|\Phi(p\Delta x,s)|^2\Phi(p\Delta x,s)\right. \\ &\left.+|\Phi(p\Delta x,q\Delta t)|^2\Phi(p\Delta x,q\Delta t))ds\right|^2 \\ &+4\sigma^2\int_{q\Delta t}^{(q+1)\Delta t}E\,|-\Phi(p\Delta x,s) + \Phi(q\Delta x,p\Delta t)|^2\,ds,\end{aligned}$$

$E|Z(\Phi)_p^q - Z|_p^q(\Phi)|^2 \to 0$ as $p\to\infty, q\to\infty$, so this proposed scheme for Φ is consistent with stochastic PDE (12).

Stability

The stability of the current scheme is shown with the help of the Von-Neumann criteria.

Von-Neumann criteria

By this method, $\Phi_{q,p}$ is replaced in the differential equation as follows,

$$\Phi_{q,p} = g(t)e^{i(\beta x)}, \tag{5}$$

and by doing some basic calculation, one get the amplification factor as follow, [13]

$$E\left|\frac{g(t+\Delta t)}{g(t)}\right|^2 \leq 1 + \chi\Delta t, \tag{6}$$

where χ is a constant.

It is a necessary and sufficient condition of stability.

Theorem 2. *The given scheme for Φ is unconditionally stable with $(q+1)\Delta t = T$ [52].*

Proof. To check the stability of the scheme, the Von-Neumann technique is used, so by linearizing Eq. (2) as follows,

$$(\iota + 2\alpha)\Phi_p^{q+1} = \alpha\Phi_{p+1}^q + \alpha\Phi_{p-1}^q + (\iota + kV_p)\Phi_p^q + \sigma\Phi_p^q(W^{(q+1)\Delta t} - W^{q\Delta t}),$$

$$(\iota + 2\alpha)g(t+\Delta t)e^{i(\beta x)} = (\alpha(e^{i(\beta\Delta x)} + e^{-i(\beta\Delta x)}) + (\iota + kV_p)) + \sigma(W^{(q+1)\Delta t} - W^{q\Delta t})g(t)e^{i(\beta x)},$$

$$E\left|\frac{g(t+\Delta t)}{g(t)}\right|^2 = \left|\frac{2\alpha - 4\alpha\sin^2(\frac{\beta\Delta x}{2}) + \iota + kV_p}{\iota + 2\alpha}\right|^2 + \left|\frac{\sigma}{\iota + 2\alpha}\right|^2 (W^{(q+1)\Delta t} - W^{q\Delta t}),$$

as maximum value of $\sin^2(\frac{\beta\Delta x}{2}) = 1$ and using Φ as the independent from the state of Winer process

$$E\left|\frac{g(t+\Delta t)}{g(t)}\right|^2 \leq \left|\frac{(\iota - 2\alpha + kV_p)}{\iota + 2\alpha}\right|^2 + \left|\frac{\sigma}{\iota + 2\alpha}\right|^2 \Delta t,$$

and $\frac{(\iota - 2\alpha + kV_p)}{\iota + 2\alpha} \leq 1$, $\frac{\sigma}{\iota + 2\alpha} = \chi$, above inequality reduces to

$$E\left|\frac{g(t+\Delta t)}{g(t)}\right|^2 \leq 1 + |\chi|^2\Delta t.$$

So, the given scheme is stable.

Convergence of the proposed scheme

The convergence of the scheme is discussed in the mean square sense.

Theorem 3. *The proposed scheme given by Eq. (2) is convergent in the mean square sense.*

Proof.

$$E\left|\Phi|_{p,q} - \Phi\right|^2 = E\left|(Z_{p,q})^{-1}(Z_{p,q}\Phi|_{p,q} - Z_{p,q}\Phi)\right|^2,$$

as proposed scheme (2) is consistent in the mean square sense i.e., $Z_{p,q}\Phi|_{p,q} \to Z_{p,q}\Phi$ as $\Delta x \to 0, \Delta t \to 0$ and $(p\Delta x, q\Delta t) \to (x,t)$,

$$E\left|(Z_{p,q})^{-1}(Z_{p,q}\Phi|_{p,q} - Z_{p,q}\Phi)\right|^2 \to 0,$$

also, as scheme is stable, then $(Z_{p,q})^{-1}$ is bounded. So, $E\left|\Phi|_{p,q} - \Phi\right|^2 \to 0$. Hence proposed scheme (2) for Φ is convergent in the mean square sense.

Remark 1. The second order accurate (in time) numerical scheme can be designed and its corresponding analysis can be carried out.

Theoretical analysis of method's

The proposed NSFD scheme is used to find the numerical approximation of the underlying model. The scheme is consistent with given equation and stability analysis is shown with the help of Von-Neumann criteria. The convergence analysis is also carried out in the mean square sense. Further for the sake of exact solutions we use Sardar subequation (SSE) and modified exponential rational (MERF) techniques that will gives us the different types of wave structures in the form of dark, bright, mixed, trigonometric, and exponential function solutions as well.

Extraction of exact solutions

Proceeding to find the exact solutions of Eq. (12), by converting PDE into ODE for by choosing the transformation $\Phi(x,t) = \Omega(\eta)e^{i(lx+mt)}$, where $\eta = \alpha x - ct$ for more detail see [53–56]. So, substituting this transformation into Eq. (12), we get the ODE form and compare real and imaginary values as follows:

$$\alpha^2\Omega''(\eta) + (m - l^2 + V(x))\Omega(\eta) + g\Omega^3(\eta) + \sigma\dot{W}(t)\Omega(\eta) = 0, \tag{7}$$

$$c\Omega'(\eta) + 2l\alpha\Omega'(\eta) = 0, \tag{8}$$

where Ω is a polynomial and $' = \frac{d}{d\eta}$.

Solutions via sardar subequation approach [57–60]

Consider only the real part of ODE eq. (real) which has the solution in the following form;

$$\Omega(\eta) = \sum_{j=0}^{N} \kappa_j\, \Theta^j(\eta), \tag{9}$$

where κ_j $(0 \leq j \leq N)$ are the constants that are found later, and $\Theta'(\eta)$ is satisfy the Eq. (7) and taking as;

$$\Theta'(\eta) = \sqrt{\gamma + \chi\Theta(\eta)^2 + \Theta(\eta)^4}, \tag{10}$$

where γ and χ are real constants. The value of N is obtained with the help of homogeneous balancing between $\Omega^3(\eta)$ and $\Omega''(\eta)$ in Eq. (7), which gives us $N = 1$. Thus, Eq. (26) takes the following form;

$$\Omega(\eta) = \kappa_0 + \kappa_1\Theta(\eta). \tag{11}$$

By substituting the Eq. (26) with its derivatives into the Eq. (7) with Eq. (27) and gathering all the terms of the same power of $\Theta^j(\eta)$. The coefficients of these polynomials equate to zero and get an algebraic system of equations. With the help of *mathematica*11.1 solving this system, we obtained the different families of solutions for the values of constant and parameters as follows:

Family-1.

$$\left\{\kappa_0 = 0; \quad \kappa_1 = \pm\frac{i\sqrt{2}\alpha}{\sqrt{g}}; \quad \chi = \frac{l^2 - m - V - \sigma W}{\alpha^2};\right.$$

The different families' solutions of Eq. (12) are extracted as;

Type-1: For $\chi = \frac{l^2 - m - V - \sigma W}{\alpha^2} > 0$ and $\gamma = 0$, then we obtained the hyperbolic solutions of Eq. (12) as follows;

$$\Phi_1^{\pm}(x,t) = \left[\pm\frac{i\sqrt{2}\alpha}{\sqrt{g}}\sqrt{-\frac{pq(l^2 - m - V - \sigma W)}{\alpha^2}} \times \mathrm{sech}_{pq}\left(\sqrt{\frac{l^2 - m - V - \sigma W}{\alpha^2}}(\alpha x - ct)\right)\right] e^{i(lx+mt)}. \tag{12}$$

$$\Phi_2^{\pm}(x,t) = \left[\pm\frac{i\sqrt{2}\alpha}{\sqrt{g}}\sqrt{\frac{pq(l^2 - m - V - \sigma W)}{\alpha^2}} \times \mathrm{csch}_{pq}\left(\sqrt{\frac{l^2 - m - V - \sigma W}{\alpha^2}}(\alpha x - ct)\right)\right] e^{i(lx+mt)}. \tag{13}$$

where $\text{sech}_{pq} = \frac{2}{pe^{\eta}+qe^{-\eta}}$ and $\text{csch}_{pq} = \frac{2}{pe^{\eta}-qe^{-\eta}}$.

Type-2: For $\chi = \frac{l^2-m-V-\sigma W}{\alpha^2} < 0$ and $\gamma = 0$, then we attained the trigonometric solutions of Eq. (12) as follows;

$$\Phi_3^{\pm}(x,t) = \left[\pm \frac{i\sqrt{2}\alpha}{\sqrt{g}} \sqrt{-\frac{pq(l^2-m-V-\sigma W)}{\alpha^2}} \times \text{sec}_{pq}\left(\sqrt{-\frac{l^2-m-V-\sigma W}{\alpha^2}}(\alpha x - ct) \right) \right] e^{i(lx+mt)}. \tag{14}$$

$$\Phi_4^{\pm}(x,t) = \left[\pm \frac{i\sqrt{2}\alpha}{\sqrt{g}} \sqrt{-\frac{pq(l^2-m-V-\sigma W)}{\alpha^2}} \times \text{csc}_{pq}\left(\sqrt{-\frac{l^2-m-V-\sigma W}{\alpha^2}}(\alpha x - ct) \right) \right] e^{i(lx+mt)}. \tag{15}$$

where $\text{sec}_{pq} = \frac{2}{pe^{i\eta}+qe^{-i\eta}}$ and $\text{csc}_{pq} = \frac{2}{pe^{i\eta}-qe^{-i\eta}}$.

Type-3: For $\chi = \frac{l^2-m-V-\sigma W}{\alpha^2} < 0$ and $\gamma = \sqrt{\frac{\chi^2}{4}}$, then we obtained the singular and dark solution of Eq. (12) as follows;

$$\Phi_5^{\pm}(x,t) = \left[\pm \frac{i\alpha}{\sqrt{g}} \sqrt{-\frac{l^2-m-V-\sigma W}{\alpha^2}} \times \tanh_{pq}\left(\frac{\sqrt{-\frac{l^2-m-V-\sigma W}{\alpha^2}}(\alpha x - ct)}{\sqrt{2}} \right) \right] e^{i(lx+mt)}. \tag{16}$$

$$\Phi_6^{\pm}(x,t) = \left[\pm \frac{i\alpha}{\sqrt{g}} \sqrt{-\frac{l^2-m-V-\sigma W}{\alpha^2}} \times \coth_{pq}\left(\frac{\sqrt{-\frac{l^2-m-V-\sigma W}{\alpha^2}}(\alpha x - ct)}{\sqrt{2}} \right) \right] e^{i(lx+mt)}. \tag{17}$$

We obtained the complex combined dark-bright solution of Eq. (12) as follows;

$$\Phi_7^{\pm}(x,t) = \left[\pm \frac{i\alpha}{\sqrt{g}} \sqrt{-\frac{l^2-m-V-\sigma W}{\alpha^2}} \times \left(\tanh_{pq}\left(\sqrt{2}\sqrt{-\frac{l^2-m-V-\sigma W}{\alpha^2}}(\alpha x - ct) \right) + i\sqrt{pq}\,\text{sech}_{pq}\left(\sqrt{2}\sqrt{-\frac{l^2-m-V-\sigma W}{\alpha^2}}(\alpha x - ct) \right) \right) \right] \times e^{i(lx+mt)}. \tag{18}$$

We obtained the mixed singular solution of Eq. (12) as follows;

$$\Phi_8^{\pm}(x,t) = \left[\pm \frac{i\alpha}{\sqrt{g}} \sqrt{-\frac{l^2-m-V-\sigma W}{\alpha^2}} \times \left(\coth_{pq}\left(\sqrt{2}\sqrt{-\frac{l^2-m-V-\sigma W}{\alpha^2}}(\alpha x - ct) \right) + \sqrt{pq}\,\text{csch}_{pq}\left(\sqrt{2}\sqrt{-\frac{l^2-m-V-\sigma W}{\alpha^2}}(\alpha x - ct) \right) \right) \right] \times e^{i(lx+mt)}. \tag{19}$$

We obtained the solitary wave solution of Eq. (12) as follows;

$$\Phi_9^{\pm}(x,t) = \left[\pm \frac{i\alpha}{2\sqrt{g}} \sqrt{-\frac{l^2-m-V-\sigma W}{\alpha^2}} \times \left(\tanh_{pq}\left(\frac{\sqrt{-\frac{l^2-m-V-\sigma W}{\alpha^2}}(\alpha x - ct)}{2\sqrt{2}} \right) + \coth_{pq}\left(\frac{\sqrt{-\frac{l^2-m-V-\sigma W}{\alpha^2}}(\alpha x - ct)}{2\sqrt{2}} \right) \right) \right] e^{i(lx+mt)}. \tag{20}$$

where $\tanh_{pq} = \frac{pe^{\eta}-qe^{-\eta}}{pe^{\eta}+qe^{-\eta}}$ and $\coth_{pq} = \frac{pe^{\eta}+qe^{-\eta}}{pe^{\eta}-qe^{-\eta}}$.

Type-4: For $\chi = \frac{l^2-m-V-\sigma W}{\alpha^2} > 0$ and $\gamma = \sqrt{\frac{\chi^2}{4}}$, then we obtained the trigonometric solution of Eq. (12) as follows;

$$\Phi_{10}^{\pm}(x,t) = \left[\pm \frac{i\alpha}{\sqrt{g}} \sqrt{\frac{l^2-m-V-\sigma W}{\alpha^2}} \times \tan_{pq}\left(\frac{\sqrt{\frac{l^2-m-V-\sigma W}{\alpha^2}}(\alpha x - ct)}{\sqrt{2}} \right) \right] e^{i(lx+mt)}. \tag{21}$$

$$\Phi_{11}^{\pm}(x,t) = \left[\pm \frac{i\alpha}{\sqrt{g}} \sqrt{\frac{l^2-m-V-\sigma W}{\alpha^2}} \times \cot_{pq}\left(\frac{\sqrt{\frac{l^2-m-V-\sigma W}{\alpha^2}}(\alpha x - ct)}{\sqrt{2}} \right) \right] e^{i(lx+mt)}. \tag{22}$$

$$\Phi_{12}^{\pm}(x,t) = \left[\pm \frac{i\alpha}{\sqrt{g}} \sqrt{\frac{l^2-m-V-\sigma W}{\alpha^2}} \times \left(\tan_{pq}\left(\sqrt{2}\sqrt{\frac{l^2-m-V-\sigma W}{\alpha^2}}(\alpha x - \nu t) \right) + \sqrt{pq}\,\text{sec}_{pq}\left(\sqrt{2}\sqrt{\frac{l^2-m-V-\sigma W}{\alpha^2}}(\alpha x - \nu t) \right) \right) \right] \times e^{i(lx+mt)}. \tag{23}$$

$$\Phi_{13}^{\pm}(x,t) = \left[\pm \frac{i\alpha}{\sqrt{g}} \sqrt{\frac{l^2-m-V-\sigma W}{\alpha^2}} \times \left(\cot_{pq}\left(\sqrt{2}\sqrt{\frac{l^2-m-V-\sigma W}{\alpha^2}}(\alpha x - \nu t) \right) + \sqrt{pq}\,\text{csc}_{pq}\left(\sqrt{2}\sqrt{\frac{l^2-m-V-\sigma W}{\alpha^2}}(\alpha x - \nu t) \right) \right) \right] \times e^{i(lx+mt)}. \tag{24}$$

$$\Phi_{14}^{\pm}(x,t) = \left[\pm \frac{i\alpha}{\sqrt{2g}} \sqrt{\frac{l^2-m-V-\sigma W}{\alpha^2}} \left(\tan_{pq}\left(\frac{\sqrt{\frac{l^2-m-V-\sigma W}{\alpha^2}}(\alpha x - ct)}{2\sqrt{2}} \right) + \cot_{pq}\left(\frac{\sqrt{\frac{l^2-m-V-\sigma W}{\alpha^2}}(\alpha x - ct)}{2\sqrt{2}} \right) \right) \right] e^{i(lx+mt)}. \tag{25}$$

where $\tan_{pq} = -i\frac{pe^{i\eta}-qe^{-i\eta}}{pe^{i\eta}+qe^{-i\eta}}$ and $\cot_{pq} = i\frac{pe^{i\eta}+qe^{-i\eta}}{pe^{i\eta}-qe^{-i\eta}}$.

Solutions via modified exponential rational function method (MERFM) [61–63]

Consider only the real part of ODE eq. (real) which has the solution in the following form;

$$\Omega(\eta) = \frac{\alpha_0 + \alpha_1\Theta(\eta) + \cdots + \alpha_N\Theta^N(\eta)}{\beta_0 + \beta_1\Theta(\eta) + \cdots + \beta_N\Theta^N(\eta)}, \tag{26}$$

where

$$\Theta(\eta) = \frac{\tau_1 e^{\lambda_1\eta} + \tau_2 e^{\lambda_2\eta}}{\tau_3 e^{\lambda_3\eta} + \tau_4 e^{\lambda_4\eta}}, \tag{27}$$

where α_j, β_j $(0 \le j \le N)$ are real unknown constants and τ_1, λ_i $(1 \le j \le 4)$ are arbitrary constants and substituting the value of N

Eq. (26) takes the following form;

$$\Omega(\eta) = \frac{\alpha_0 + \alpha_1 \Theta(\eta)}{\beta_0 + \beta_1 \Theta(\eta)}. \tag{28}$$

By substituting the Eq. (26) with its derivatives into the Eq. (7) with Eq. (27) and gathering all the terms of the same power of $e^{\lambda_j \eta}$ with (j = 1,2,3,4). The coefficients of these polynomials equate to zero and get an algebraic system of equations. With the help of *mathematica*11.1 solving this system, we obtained the different families of solutions for the values of constant and parameters as follows:

Case-1. When $\tau = [-1,-1,1-1]$ and $\lambda = [1,-1,1,-1]$, then we obtained

$$\Omega(\eta) = -\frac{\cosh(\eta)}{\sinh(\eta)}. \tag{29}$$

The dark solitons solution Eq. (12) are derived as follows;

Family-1.

$$\left\{\alpha_0 = -\frac{i\sqrt{2}\alpha\beta_1}{\sqrt{g}};\quad \alpha_1 = -\frac{i\sqrt{2}\alpha\beta_0}{\sqrt{g}};\quad m = 2\alpha^2 + l^2 - V - \sigma W;\right.$$

$$\Phi_{15}(x,t) = \left(\frac{\left(-\frac{i\sqrt{2}\alpha\beta_0 \coth(ct-\alpha x)}{\sqrt{g}} - \frac{i\sqrt{2}\alpha\beta_1}{\sqrt{g}}\right)}{\beta_0 + \beta_1 \coth(ct-\alpha x)}\right) e^{i\left(t\left(2\alpha^2 + l^2 - V - \sigma W\right) + lx\right)}, \tag{30}$$

Family-2.

$$\left\{\alpha_0 = 0;\quad \alpha_1 = -\frac{i\sqrt{2}\alpha\beta_0}{\sqrt{g}};\quad \beta_0 = \beta_0;\quad \beta_1 = 0;\quad m = 2\alpha^2 + l^2 - V - \sigma W;\right.$$

$$\Phi_{16}(x,t) = \left(\frac{i\sqrt{2}\alpha \coth(\eta)}{\sqrt{g}}\right) e^{i\left(t\left(2\alpha^2 + l^2 - V - \sigma W\right) + lx\right)}, \tag{31}$$

Case-2. When $\tau = [2,0,1-1]$ and $\lambda = [1,0,1,-1]$, then we obtained

$$\Omega(\eta) = \frac{\sinh(\eta) + \cosh(\eta)}{\sinh(\eta)}. \tag{32}$$

The wave solutions of Eq. (12) are derived as follows;

Family-1.

$$\left\{\alpha_0 = \frac{i\sqrt{2}\alpha\beta_0}{\sqrt{g}};\quad \alpha_1 = -\frac{i\alpha\beta_0}{\sqrt{2}\sqrt{g}};\quad \beta_1 = -\frac{\beta_0}{2};\quad m = 2\alpha^2 + l^2 - V - \sigma W;\right.$$

$$\Phi_{17}(x,t) = \left(\frac{\left(\frac{i\alpha\beta_0 \operatorname{csch}(ct-\alpha x)(\cosh(ct-\alpha x) - \sinh(ct-\alpha x))}{\sqrt{2}\sqrt{g}} + \frac{i\sqrt{2}\alpha\beta_0}{\sqrt{g}}\right)}{\beta_0 + \frac{1}{2}\beta_0 \operatorname{csch}(ct-\alpha x)(\cosh(ct-\alpha x) - \sinh(ct-\alpha x))}\right) \times e^{i\left(t\left(2\alpha^2 + l^2 - V - \sigma W\right) + lx\right)}, \tag{33}$$

Family-2.

$$\left\{\alpha_0 = \frac{i\sqrt{2}\alpha\beta_0}{\sqrt{g}};\quad \alpha_1 = -\frac{i\sqrt{2}\alpha(\beta_0+\beta_1)}{\sqrt{g}};\quad m = 2\alpha^2 + l^2 - V - \sigma W;\right.$$

$$\Phi_{18}(x,t) = \left(\frac{\left(\frac{i\sqrt{2}\alpha(\beta_0+\beta_1) \operatorname{csch}(ct-\alpha x)(\cosh(ct-\alpha x) - \sinh(ct-\alpha x))}{\sqrt{g}} + \frac{i\sqrt{2}\alpha\beta_0}{\sqrt{g}}\right)}{\beta_0 - \beta_1 \operatorname{csch}(ct-\alpha x)(\cosh(ct-\alpha x) - \sinh(ct-\alpha x))}\right) \times e^{i\left(t\left(2\alpha^2 + l^2 - V - \sigma W\right) + lx\right)}, \tag{34}$$

Family-3.

$$\left\{\alpha_1 = -\frac{\alpha_0}{2};\quad \beta_1 = -\frac{\beta_0}{2};\quad m = \frac{\alpha_0^2(-g) + \beta_0^2 l^2 - \beta_0^2 V - \beta_0^2 \sigma W}{\beta_0^2};\right.$$

$$\Phi_{19}(x,t) = \left(\frac{\left(\alpha_0 + \frac{1}{2}\alpha_0 \operatorname{csch}(ct-\alpha x)(\cosh(ct-\alpha x) - \sinh(ct-\alpha x))\right)}{\beta_0 + \frac{1}{2}\beta_0 \operatorname{csch}(ct-\alpha x)(\cosh(ct-\alpha x) - \sinh(ct-\alpha x))}\right) \times e^{i\left(\frac{t\left(\alpha_0^2(-g) + \beta_0^2 l^2 - \beta_0^2 V - \beta_0^2 \sigma W\right)}{\beta_0^2} + lx\right)}, \tag{35}$$

Case-3. When $\tau = [-1-i, 1-i, -1, 1]$ and $\lambda = [i, -i, i, -i]$, then we obtained

$$\Omega(\eta) = \frac{\sin(\eta) + \cos(\eta)}{\sin(\eta)}. \tag{36}$$

The wave solutions of Eq. (12) are derived as follows;

Family-1.

$$\left\{\alpha_0 = (-1-i)\alpha_1;\quad \beta_0 = (-1-i)\beta_1;\quad m = \frac{\alpha_1^2(-g) + \beta_1^2 l^2 - \beta_1^2 V - \beta_1^2 \sigma W}{\beta_1^2};\right.$$

$$\Phi_{20}(x,t) = \left(\frac{\left(-\alpha_1 \csc(ct-\alpha x)(\cos(ct-\alpha x) - \sin(ct-\alpha x)) + (-1-i)\alpha_1\right)}{-\beta_1 \csc(ct-\alpha x)(\cos(ct-\alpha x) - \sin(ct-\alpha x)) + (-1-i)\beta_1}\right) \times e^{i\left(\frac{t\left(\alpha_1^2(-g) + \beta_1^2 l^2 - \beta_1^2 V - \beta_1^2 \sigma W\right)}{\beta_1^2} + lx\right)}, \tag{37}$$

Family-2.

$$\left\{\alpha_0 = \frac{i\sqrt{2}\alpha\beta_0}{\sqrt{g}};\quad \alpha_1 = -\frac{i\sqrt{2}\alpha\beta_0}{\sqrt{g}};\quad \beta_1 = 0;\quad m = -2\alpha^2 + l^2 - V - \sigma W;\right.$$

$$\Phi_{21}(x,t) = \left(\frac{\left(\frac{i\sqrt{2}\alpha\beta_0 \csc(ct-\alpha x)(\cos(ct-\alpha x) - \sin(ct-\alpha x))}{\sqrt{g}} + \frac{i\sqrt{2}\alpha\beta_0}{\sqrt{g}}\right)}{\beta_0}\right) \times e^{i\left(t\left(-2\alpha^2 + l^2 - V - \sigma W\right) + lx\right)}, \tag{38}$$

Family-3.

$$\left\{\alpha_0 = -\frac{i\sqrt{2}\alpha\beta_1}{\sqrt{g}};\quad \alpha_1 = 0;\quad \beta_0 = -\beta_1;\quad m = -2\alpha^2 + l^2 - V - \sigma W;\right.$$

$$\Phi_{22}(x,t) = \left(-\frac{i\sqrt{2}\alpha\beta_1}{\sqrt{g}\left(\beta_1(-\csc(ct-\alpha x))(\cos(ct-\alpha x) - \sin(ct-\alpha x)) - \beta_1\right)}\right) \times e^{i\left(t\left(-2\alpha^2 + l^2 - V - \sigma W\right) + lx\right)}. \tag{39}$$

Case-4. When $\tau = [2,0,1,1]$ and $\lambda = [-1,0,1,-1]$, then we obtained

$$\Omega(\eta) = \frac{\cosh(\eta) + \sinh(\eta)}{\cosh(\eta)}. \tag{40}$$

The soliton solutions of Eq. (12) are derived as follows;

Family-1.

$$\left\{\alpha_0 = \frac{i\sqrt{2}\alpha\beta_0}{\sqrt{g}};\quad \alpha_1 = -\frac{i\alpha\beta_0}{\sqrt{2}\sqrt{g}};\quad \beta_1 = -\frac{\beta_0}{2}; m = 2\alpha^2 + l^2 - V - \sigma W;\right.$$

$$\Phi_{23}(x,t) = \left(\frac{\frac{i\sqrt{2}\alpha\beta_0}{\sqrt{g}} - \frac{i\alpha\beta_0 \operatorname{sech}(ct-\alpha x)(\sinh(ct-\alpha x) + \cosh(ct-\alpha x))}{\sqrt{2}\sqrt{g}}}{\beta_0 - \frac{1}{2}\beta_0 \operatorname{sech}(ct-\alpha x)(\sinh(ct-\alpha x) + \cosh(ct-\alpha x))}\right) \times e^{i\left(t\left(-2\alpha^2 + l^2 - V - \sigma W\right) + lx\right)}, \tag{41}$$

Family-2.

$$\left\{\alpha_0 = -\frac{i\sqrt{2}\alpha\beta_0}{\sqrt{g}}; \alpha_1 = \frac{i\sqrt{2}\alpha\beta_0}{\sqrt{g}}; \beta_1 = 0; m = 2\alpha^2 + l^2 - V - \sigma W;\right.$$

$$\Phi_{24}(x,t) = \left(\frac{\left(\frac{i\sqrt{2}\alpha\beta_0 \operatorname{sech}(ct-\alpha x)(\sinh(ct-\alpha x) + \cosh(ct-\alpha x))}{\sqrt{g}} - \frac{i\sqrt{2}\alpha\beta_0}{\sqrt{g}}\right)}{\beta_0}\right) \times e^{i\left(t\left(2\alpha^2 + l^2 - V - \sigma W\right) + lx\right)}. \tag{42}$$

Case-5. When $\tau = [-3,-2,1,1]$ and $\lambda = [0,1,0,1]$, then we obtained

$$\Omega(\eta) = \frac{-2e^{\eta} - 3}{e^{\eta} + 1}. \tag{43}$$

The wave solutions of Eq. (12) are derived as follows;

Family-1.

$$\left\{\alpha_1=\frac{\alpha_0}{3};\quad \beta_1=\frac{\beta_0}{3};\quad m=\frac{\alpha_0^2(-g)+\beta_0^2l^2-\beta_0^2V-\beta_0^2\sigma W}{\beta_0^2};\right.$$

$$\Phi_{25}(x,t)=\left(\frac{\left(\alpha_0+\frac{\alpha_0\left(-2e^{\alpha x-ct}-3\right)}{3\left(e^{\alpha x-ct}+1\right)}\right)}{\beta_0+\frac{\beta_0\left(-2e^{\alpha x-ct}-3\right)}{3\left(e^{\alpha x-ct}+1\right)}}\right)e^{i\left(\frac{t\left(\alpha_0^2(-g)+\beta_0^2l^2-\beta_0^2V-\beta_0^2\sigma W\right)}{\beta_0^2}+lx\right)},\tag{44}$$

Family-2.

$$\left\{\alpha_0=\frac{6i\sqrt{2}\alpha\beta_1}{\sqrt{g}};\quad \alpha_1=\frac{5i\alpha\beta_1}{\sqrt{2}\sqrt{g}};\quad \beta_0=0;\quad m=\frac{1}{2}\left(\alpha^2+2l^2-2V-2\sigma W\right);\right.$$

$$\Phi_{26}(x,t)=\left(\frac{\left(e^{\alpha x-ct}+1\right)\left(\frac{5i\alpha\beta_1\left(-2e^{\alpha x-ct}-3\right)}{\sqrt{2}\sqrt{g}\left(e^{\alpha x-ct}+1\right)}+\frac{6i\sqrt{2}\alpha\beta_1}{\sqrt{g}}\right)e^{i\left(\frac{1}{2}t\left(\alpha^2+2l^2-2V-2\sigma W\right)+lx\right)}}{\beta_1\left(-2e^{\alpha x-ct}-3\right)}\right),\tag{45}$$

Family-3.

$$\left\{\alpha_0=0;\quad \alpha_1=-\frac{i\alpha\beta_0}{12\sqrt{2}\sqrt{g}};\quad \beta_1=\frac{5\beta_0}{12};\quad m=\frac{1}{2}\left(\alpha^2+2l^2-2V-2\sigma W\right);\right.$$

$$\Phi_{27}(x,t)=\left(-\frac{i\alpha\beta_0\left(-2e^{\alpha x-ct}-3\right)}{12\sqrt{2}\sqrt{g}\left(e^{\alpha x-ct}+1\right)\left(\beta_0+\frac{5\beta_0\left(-2e^{\alpha x-ct}-3\right)}{12\left(e^{\alpha x-ct}+1\right)}\right)}\right)\times e^{i\left(\frac{1}{2}t\left(\alpha^2+2l^2-2V-2\sigma W\right)+lx\right)}.\tag{46}$$

Case-6. When $\tau=[3,2,1,1]$ and $\lambda=[0,1,0,1]$, then we obtained

$$\Omega(\eta)=\frac{3e^{\eta}+2}{e^{\eta}+1}.\tag{47}$$

The soliton-like solutions of Eq. (12) are derived as follows;

Family-1.

$$\left\{\alpha_0=-\frac{6i\sqrt{2}\alpha\beta_1}{\sqrt{g}};\quad \alpha_1=\frac{5i\alpha\beta_1}{\sqrt{2}\sqrt{g}};\quad \beta_0=0;\right.$$
$$\left.m=\frac{1}{2}\left(\alpha^2+2l^2-2V-2\sigma W\right);\right.$$

$$\Phi_{28}(x,t)=\left(\frac{\left(e^{\alpha x-ct}+1\right)\left(\frac{5i\alpha\beta_1\left(3e^{\alpha x-ct}+2\right)}{\sqrt{2}\sqrt{g}\left(e^{\alpha x-ct}+1\right)}-\frac{6i\sqrt{2}\alpha\beta_1}{\sqrt{g}}\right)}{\beta_1\left(3e^{\alpha x-ct}+2\right)}\right)\times e^{i\left(\frac{1}{2}t\left(\alpha^2+2l^2-2V-2\sigma W\right)+lx\right)},\tag{48}$$

Family-2.

$$\left\{\alpha_1=-\frac{1}{12}\left(5\alpha_0\right);\quad \beta_1=-\frac{1}{12}\left(5\beta_0\right);\quad m=\frac{\alpha_0^2(-g)+\beta_0^2l^2-\beta_0^2V-\beta_0^2\sigma W}{\beta_0^2};\right.$$

$$\Phi_{29}(x,t)=\left(\frac{\left(\alpha_0-\frac{5\alpha_0\left(3e^{\alpha x-ct}+2\right)}{12\left(e^{\alpha x-ct}+1\right)}\right)}{\beta_0-\frac{5\beta_0\left(3e^{\alpha x-ct}+2\right)}{12\left(e^{\alpha x-ct}+1\right)}}\right)e^{i\left(\frac{t\left(\alpha_0^2(-g)+\beta_0^2l^2-\beta_0^2V-\beta_0^2\sigma W\right)}{\beta_0^2}+lx\right)},\tag{49}$$

Comparison of plots

In this section, the graphical comparison of numerical solutions and exact solutions are drawn,

Example 1. The test problem is considered as follows,

$$i\Phi_t=-\frac{1}{2}\Phi_{xx}+V(x)\Phi+g|\Phi|^2\Phi+\sigma\dot{W}(t)\Phi,\tag{50}$$

using the initial condition as

$$\Phi(x,0)=(-3.35819+0.i)e^{i(2.95x+0.)}\text{sech}(0.793915(2.991x+0.)),\tag{51}$$

and BCs as follows,

$$\Phi(0,t)=(-3.35819+0.i)e^{i(1.91t+0.)}\text{sech}(0.793915(0.-0.09t)),\tag{52}$$

$$\Phi(1,t)=(-3.35819+0.i)e^{i(1.91t+2.95)}\text{sech}(0.793915(2.991-0.09t)).\tag{53}$$

We construct the graphs of NFDS from Eq. (2) using the above IC and BCs and compare them with the exact solution from the Eq. (12). So, Fig. 1 shows the graphical comparison of NSFD with exact solution $\Phi_1(x,t)$.

Example 2. The test problem is considered as follows,

$$i\Phi_t=-\frac{1}{2}\Phi_{xx}+V(x)\Phi+g|\Phi|^2\Phi+\sigma\dot{W}(t)\Phi,\tag{54}$$

using the initial condition as

$$\Phi(x,0)=(-3.00688+0.i)e^{i(2.95x+0.)}\text{sech}((0.710861+0.i)(2.991x+0.)),\tag{55}$$

and BCs as follows,

$$\Phi(0,t)=(-3.00688+0.i)e^{i(2.91t+0.)}\text{sech}((0.710861+0.i)(0.-0.9t)),\tag{56}$$

$$\Phi(1,t)=(-3.00688+0.i)e^{i(2.91t+2.95)}\text{sech}((0.710861+0.i)(2.991-0.9t)).\tag{57}$$

We construct the graphs of NFDS from Eq. (2) using the above IC and BCs and compare them with the exact solution from the Eq. (14). So, Fig. 2 shows the graphical comparison of NSFD with exact solution $\Phi_3(x,t)$.

Example 3. The test problem is considered as follows,

$$i\Phi_t=-\frac{1}{2}\Phi_{xx}+V(x)\Phi+g|\Phi|^2\Phi+\sigma\dot{W}(t)\Phi,\tag{58}$$

using the initial condition as

$$\Phi(x,0)=(0.+1.52948i)e^{i(0.905x+0.)}\tanh(0.566234(1.91x+0.)),\tag{59}$$

and BCs as follows,

$$\Phi(0,t)=(0.+1.52948i)e^{i(1.9091t+0.)}\tanh(0.566234(0.-1.9t)),\tag{60}$$

$$\Phi(1,t)=(0.+1.52948i)e^{i(1.9091t+0.905)}\tanh(0.566234(1.91-1.9t)).\tag{61}$$

We construct the graphs of NFDS from Eq. (2) using the above IC and BCs and compare them with the exact solution from the Eq. (28). So, Fig. 3 shows the graphical comparison of NSFD with exact solution $\Phi_5(x,t)$.

Example 4. The test problem is considered as follows,

$$i\Phi_t=-\frac{1}{2}\Phi_{xx}+V(x)\Phi+g|\Phi|^2\Phi+\sigma\dot{W}(t)\Phi,\tag{62}$$

using the initial condition as

$$\Phi(x,0)=(0.+2.08475i)e^{i(2.5x+0.)}\tan(0.506577(2.91x+0.)),\tag{63}$$

and BCs as follows,

$$\Phi(0,t)=(0.+2.08475i)e^{i(0.91t+0.)}\tan(0.506577(0.-1.9t)),\tag{64}$$

$$\Phi(1,t)=(0.+2.08475i)e^{i(0.91t+2.5)}\tan(0.506577(2.91-1.9t)).\tag{65}$$

We construct the graphs of NFDS from Eq. (2) using the above IC and BCs and compare them with the exact solution from the Eq. (21). So, Fig. 4 shows the graphical comparison of NSFD with exact solution $\Phi_{10}(x,t)$.

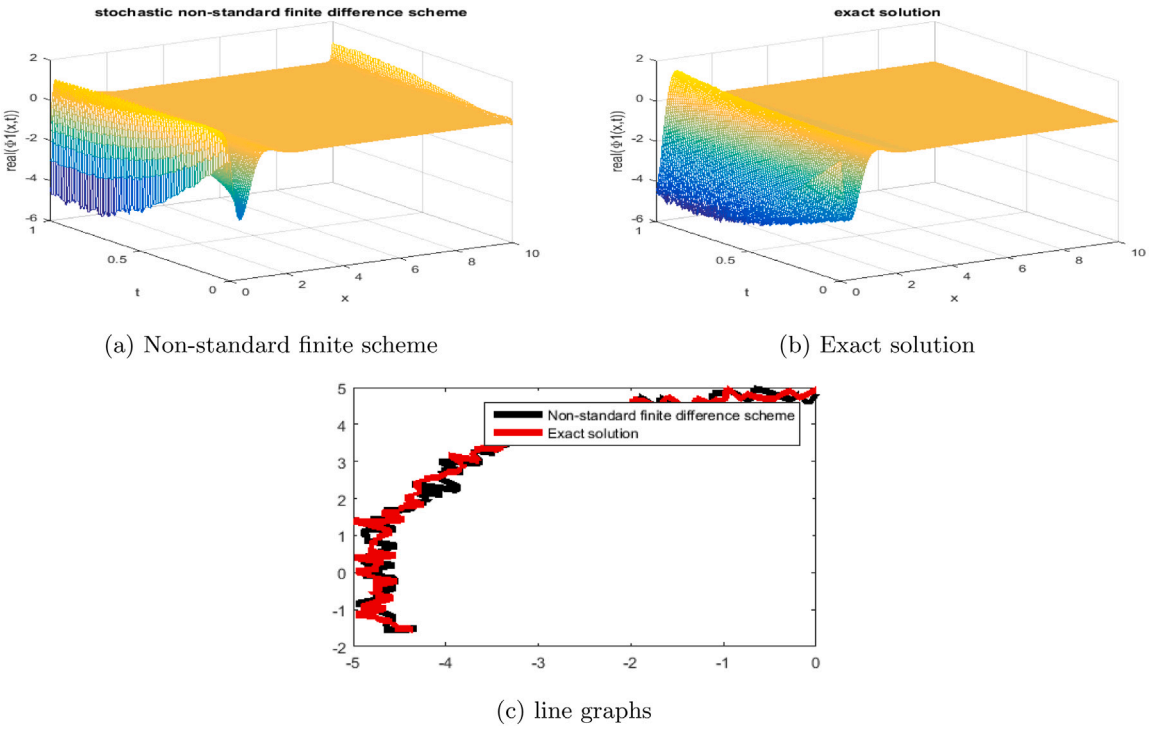

(a) Non-standard finite scheme (b) Exact solution

(c) line graphs

Fig. 1. The subfig (a) for non-standard finite difference scheme, subfig (b) for the exact solution $\Phi_1(x,t)$ and subfig (c) shows the line comparison for both (a) and (b) subfigs using the parameters values that are given in Appendix "Graphics parameters".

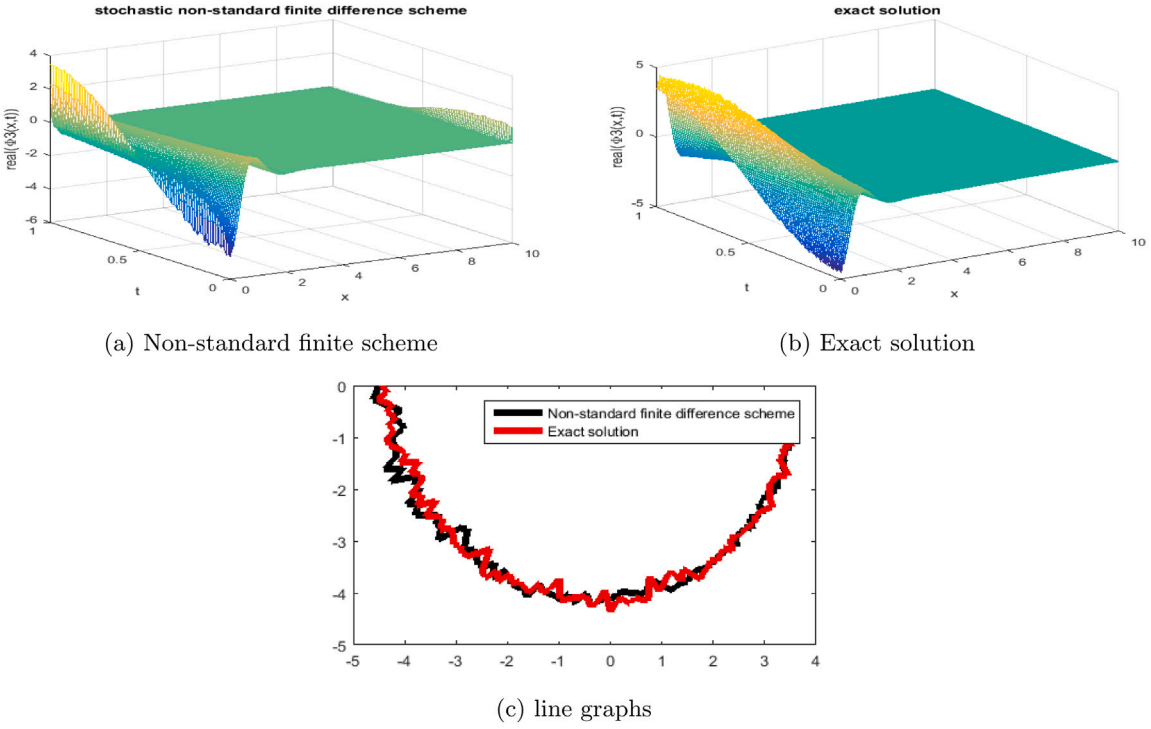

(a) Non-standard finite scheme (b) Exact solution

(c) line graphs

Fig. 2. The subfig (a) for non-standard finite difference scheme, subfig (b) for the exact solution $\Phi_3(x,t)$ and subfig (c) shows the line comparison for both (a) and (b) subfigs using the parameters values that are given in Appendix "Graphics parameters".

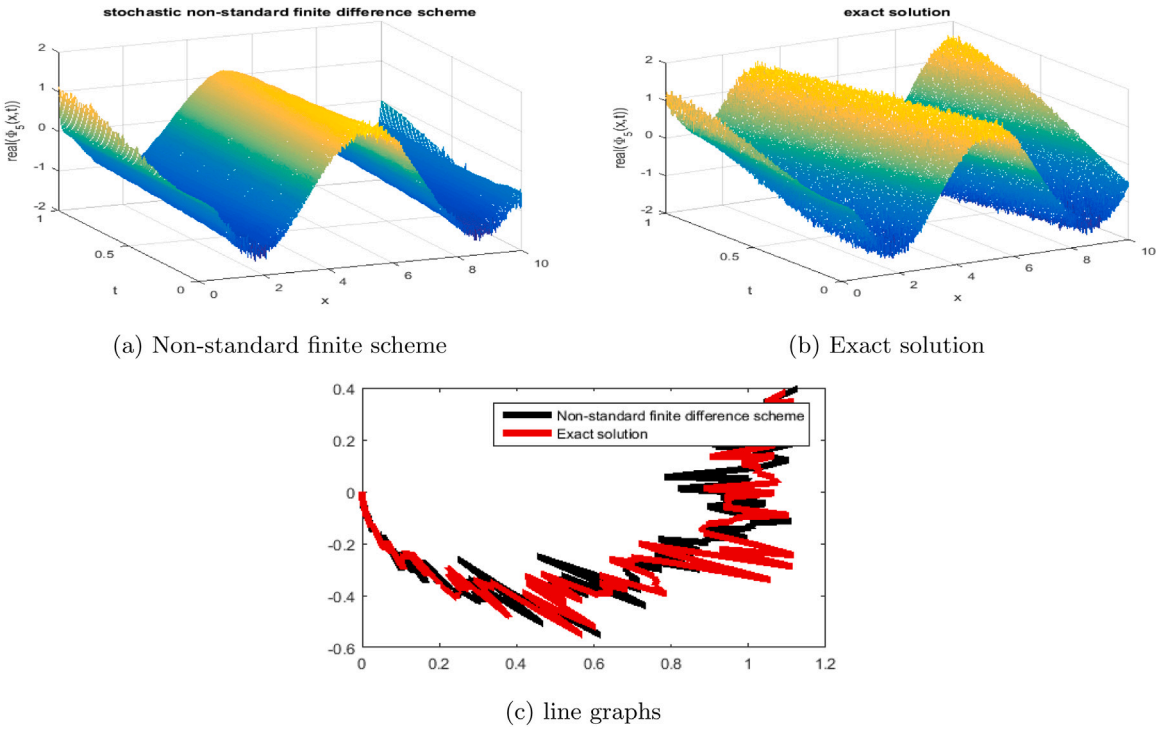

Fig. 3. The subfig (a) for non-standard finite difference scheme, subfig (b) for the exact solution $\Phi_5(x,t)$ and subfig (c) shows the line comparison for both (a) and (b) subfigs using the parameters' values that are given in Appendix "Graphics parameters".

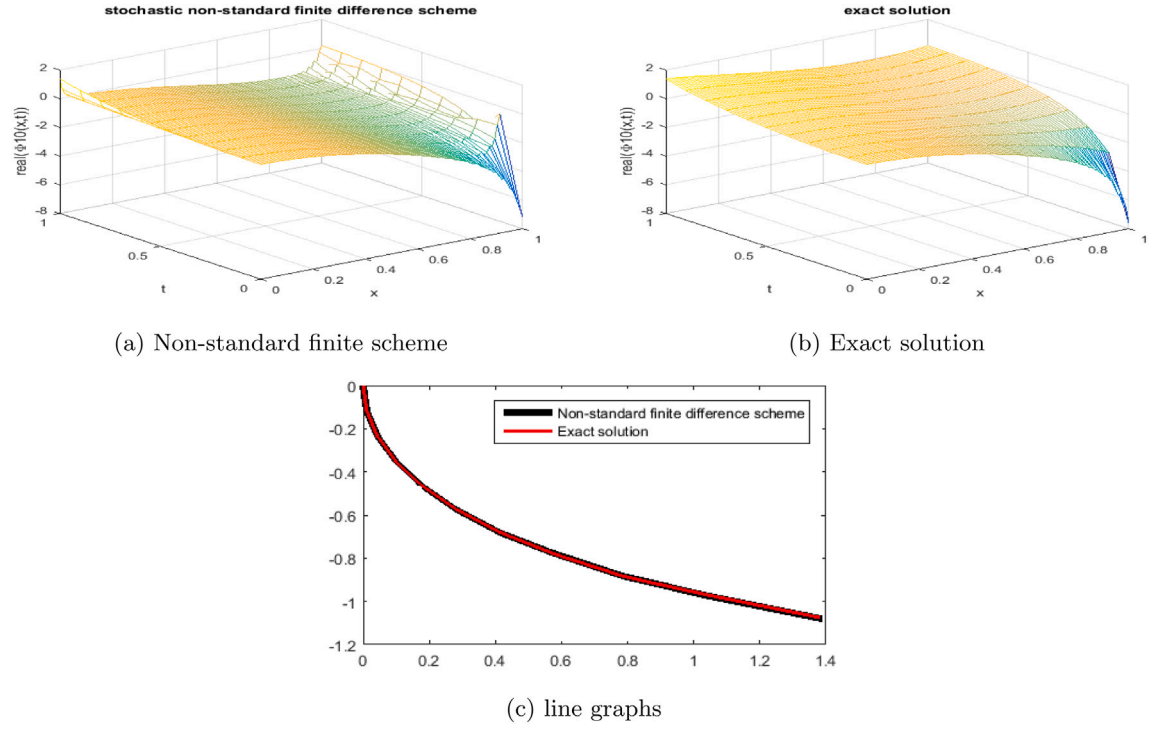

Fig. 4. The subfig (a) for non-standard finite difference scheme, subfig (b) for the exact solution $\Phi_{10}(x,t)$ and subfig (c) shows the line comparison for both (a) and (b) subfigs using the parameters values that are given in Appendix "Graphics parameters".

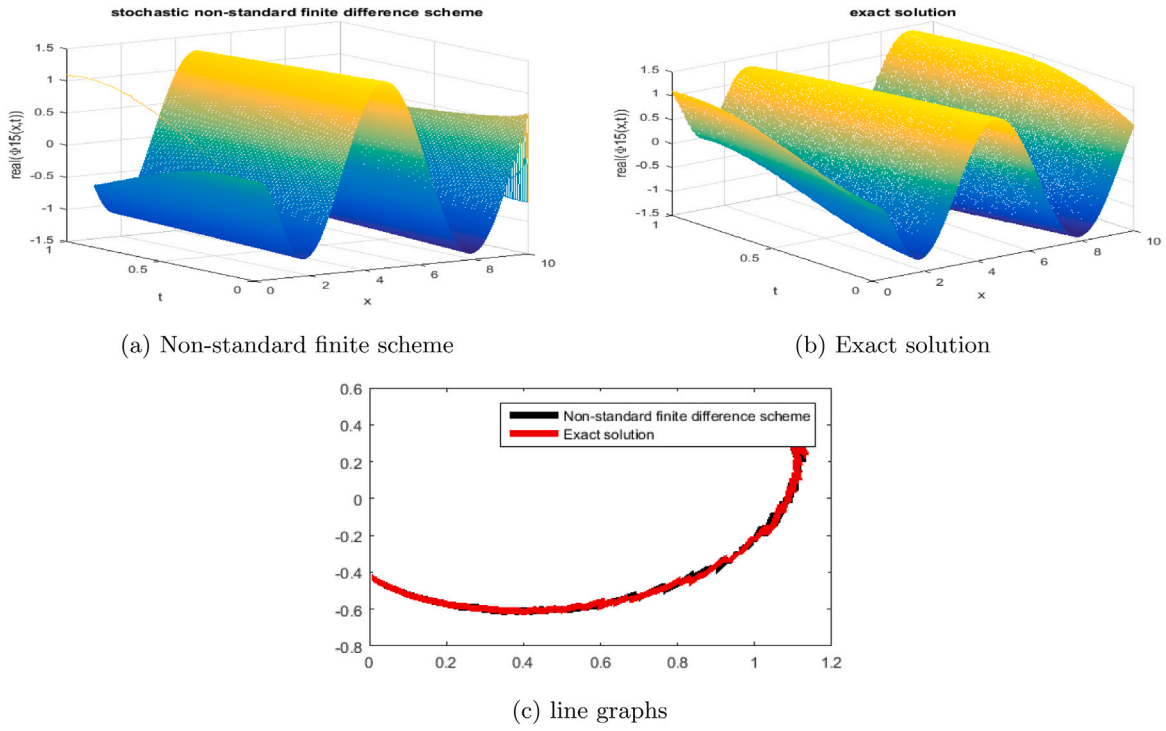

(a) Non-standard finite scheme (b) Exact solution

(c) line graphs

Fig. 5. The subfig (a) for non-standard finite difference scheme, subfig (b) for the exact solution $\Phi_{15}(x,t)$ and subfig (c) shows the line comparison for both (a) and (b) subfigs using the parameters values that are given in Appendix "Graphics parameters".

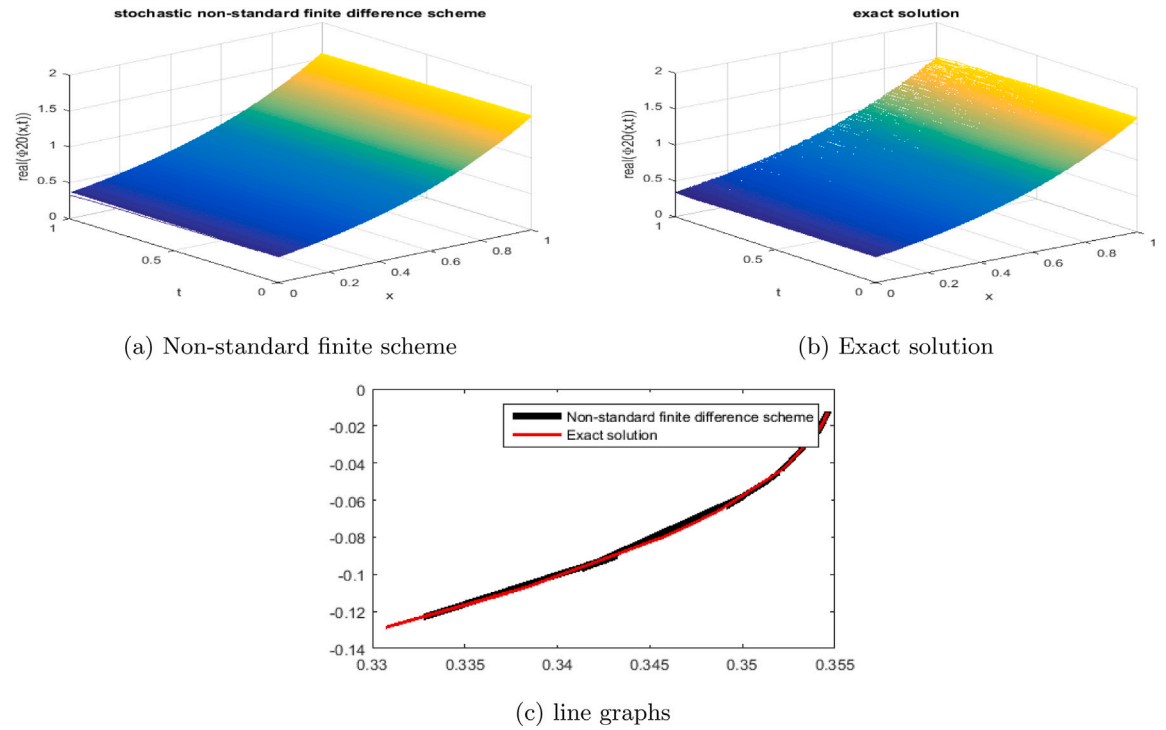

(a) Non-standard finite scheme (b) Exact solution

(c) line graphs

Fig. 6. The subfig (a) for non-standard finite difference scheme, subfig (b) for the exact solution $\Phi_{20}(x,t)$ and subfig (c) shows the line comparison for both (a) and (b) subfigs using the parameters values that are given in Appendix "Graphics parameters".

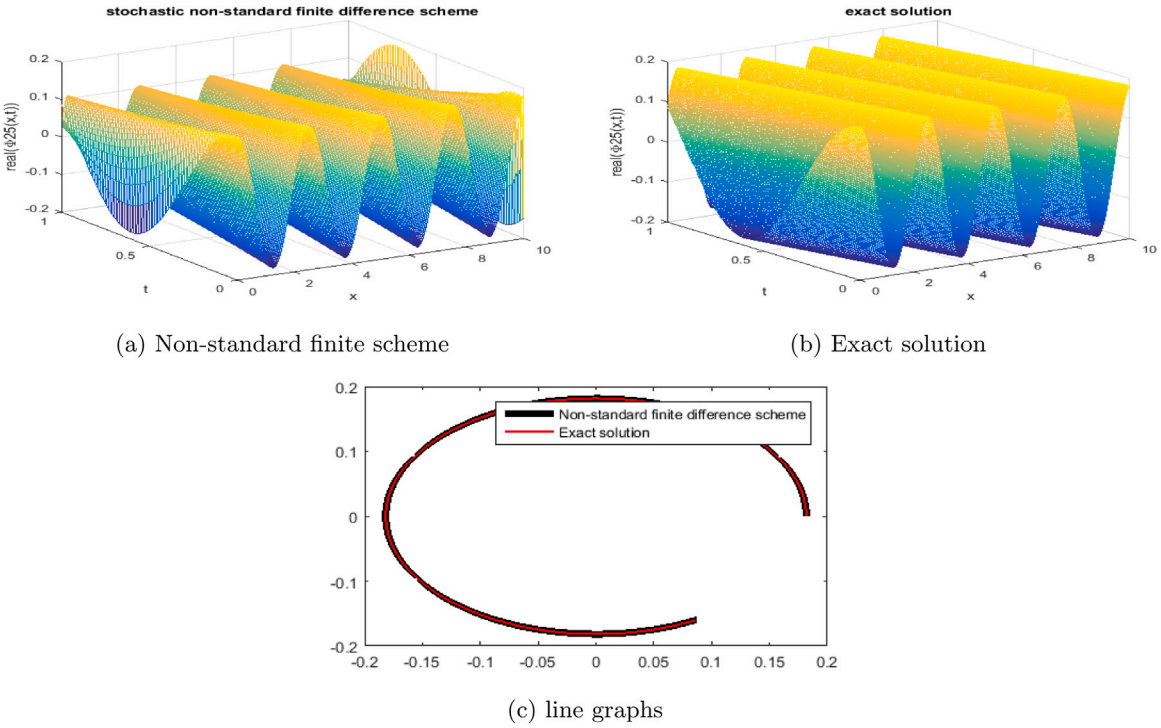

(a) Non-standard finite scheme (b) Exact solution

(c) line graphs

Fig. 7. The subfig (a) for non-standard finite difference scheme, subfig (b) for the exact solution $\Phi_{25}(x,t)$ and subfig (c) shows the line comparison for both (a) and (b) subfigs using the parameters values that are given in Appendix "Graphics parameters".

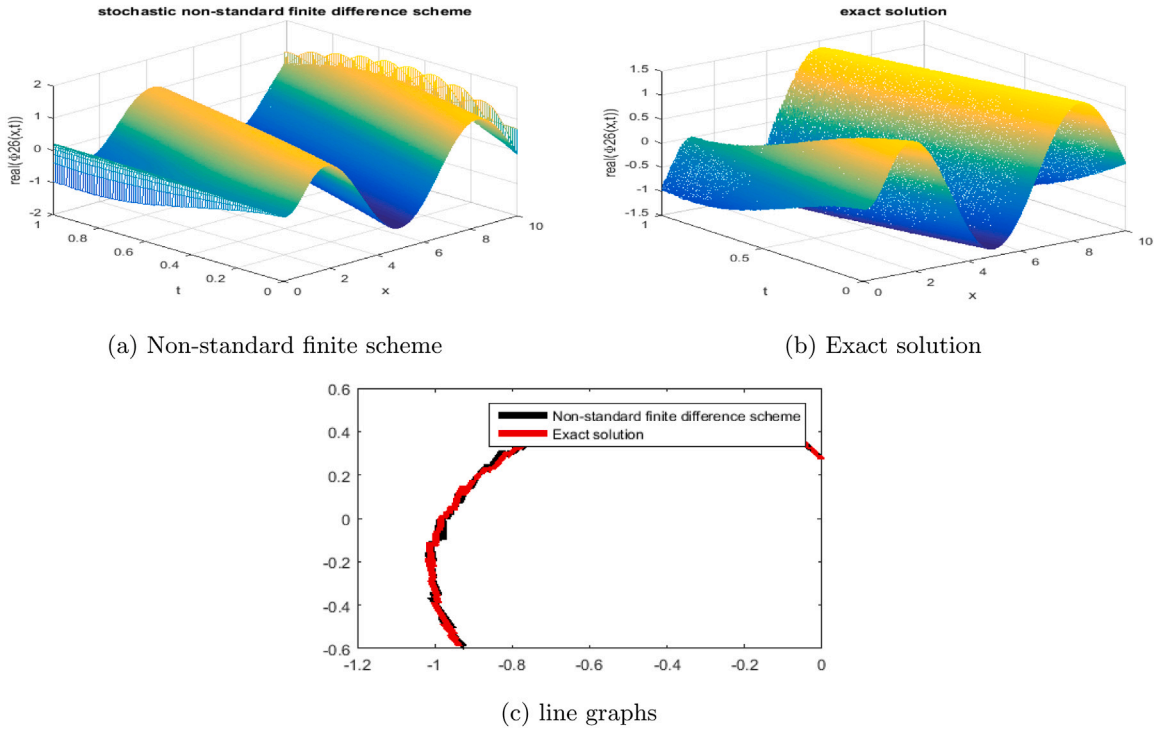

(a) Non-standard finite scheme (b) Exact solution

(c) line graphs

Fig. 8. The subfig (a) for non-standard finite difference scheme, subfig (b) for the exact solution $\Phi_{26}(x,t)$ and subfig (c) shows the line comparison for both (a) and (b) subfigs using the parameters values that are given in Appendix "Graphics parameters".

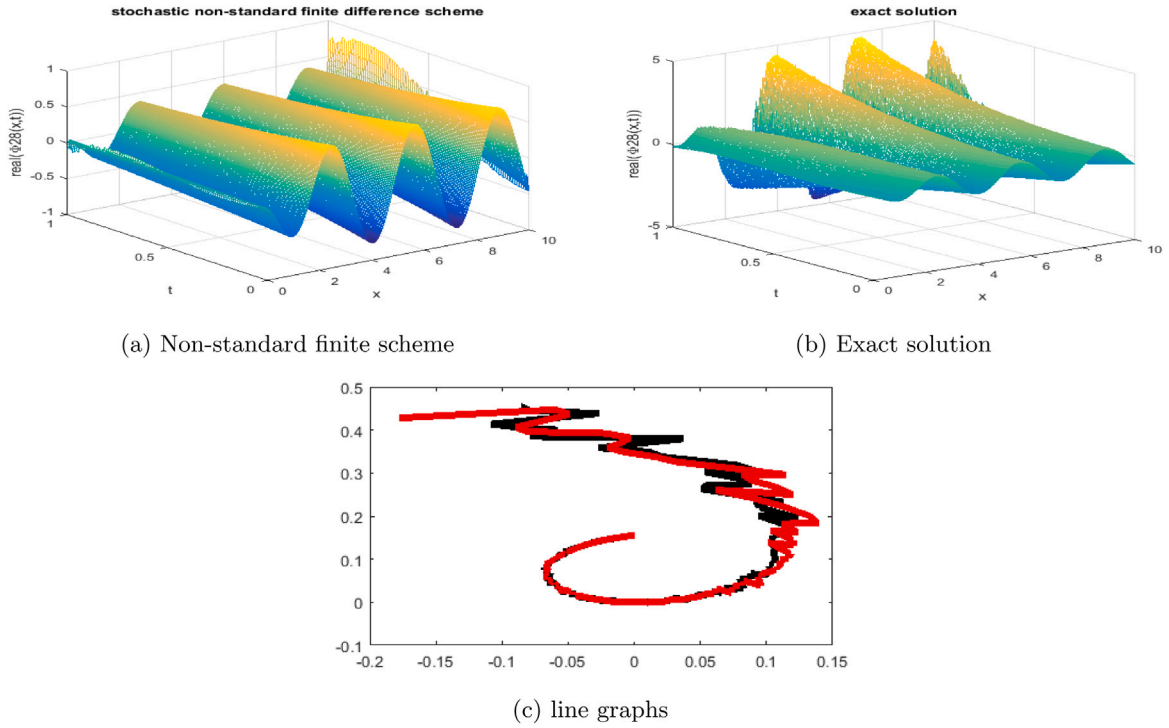

(a) Non-standard finite scheme (b) Exact solution

(c) line graphs

Fig. 9. The subfig (a) for non-standard finite difference scheme, subfig (b) for the exact solution $\Phi_{28}(x,t)$ and subfig (c) shows the line comparison for both (a) and (b) subfigs using the parameters values that are given in Appendix "Graphics parameters".

Example 5. The test problem is considered as follows,

$$i\Phi_t = -\frac{1}{2}\Phi_{xx} + V(x)\Phi + g|\Phi|^2\Phi + \sigma\dot{W}(t)\Phi, \tag{66}$$

using the initial condition as

$$\Phi(x,0) = \frac{e^{i(0.995x+0.)}((0.-4.20446i)-(0.+1.26134i)\coth(0.-0.991x))}{3\coth(0.-0.991x)+0.9}, \tag{67}$$

and BCs as follows,

$$\Phi(0,t) = \frac{e^{i(2.01991t+0.)}((0.-4.20446i)-(0.+1.26134i)\coth(0.9t+0.))}{3\coth(0.9t+0.)+0.9}, \tag{68}$$

$$\Phi(1,t) = \frac{e^{i(2.01991t+0.995)}((0.+1.26134i)\coth(0.991-0.9t)+(0.-4.20446i))}{0.9-3\coth(0.991-0.9t)}. \tag{69}$$

We construct the graphs of NFDS from Eq. (2) using the above IC and BCs and compare them with the exact solution from the Eq. (30). So, Fig. 5 shows the graphical comparison of NSFD with exact solution $\Phi_{15}(x,t)$.

Example 6. The test problem is considered as follows,

$$i\Phi_t = -\frac{1}{2}\Phi_{xx} + V(x)\Phi + g|\Phi|^2\Phi + \sigma\dot{W}(t)\Phi, \tag{70}$$

using the initial condition as

$$\Phi(x,0) = \frac{e^{i(1.5x+0.)}(-1.1\csc(0.-3.91x)(\cos(0.-3.91x)-\sin(0.-3.91x))+(-1.1-1.1i))}{-3.1\csc(0.-3.91x)(\cos(0.-3.91x)-\sin(0.-3.91x))+(-3.1-3.1i)}, \tag{71}$$

and BCs as follows,

$$\Phi(0,t) = \frac{e^{i(1.15725t+0.)}(-1.1\csc(1.9t+0.)(\cos(1.9t+0.)-\sin(1.9t+0.))+(-1.1-1.1i))}{-3.1\csc(1.9t+0.)(\cos(1.9t+0.)-\sin(1.9t+0.))+(-3.1-3.1i)}, \tag{72}$$

$$\Phi(1,t) = \frac{e^{i(1.15725t+1.5)}(1.1\csc(3.91-1.9t)(\sin(3.91-1.9t)+\cos(3.91-1.9t))+(-1.1-1.1i))}{3.1\csc(3.91-1.9t)(\sin(3.91-1.9t)+\cos(3.91-1.9t))+(-3.1-3.1i)}. \tag{73}$$

We construct the graphs of NFDS from Eq. (2) using the above IC and BCs and compare them with the exact solution from the Eq. (37). So, Fig. 6 shows the graphical comparison of NSFD with exact solution $\Phi_{20}(x,t)$.

Example 7. The test problem is considered as follows,

$$i\Phi_t = -\frac{1}{2}\Phi_{xx} + V(x)\Phi + g|\Phi|^2\Phi + \sigma\dot{W}(t)\Phi, \tag{74}$$

using the initial condition as

$$\Phi(x,0) = 0.181818e^{(0.+2.5i)x}, \tag{75}$$

and BCs as follows,

$$\Phi(0,t) = 0.181818e^{(0.+5.20733i)t}, \tag{76}$$

$$\Phi(1,t) = 0.181818e^{(0.+5.20733i)t+(0.+2.5i)}. \tag{77}$$

We construct the graphs of NFDS from Eq. (2) using the above IC and BCs and compare them with the exact solution from the Eq. (44). So, Fig. 7 shows the graphical comparison of NSFD with exact solution $\Phi_{25}(x,t)$.

Example 8. The test problem is considered as follows,

$$i\Phi_t = -\frac{1}{2}\Phi_{xx} + V(x)\Phi + g|\Phi|^2\Phi + \sigma\dot{W}(t)\Phi, \tag{78}$$

using the initial condition as

$$\Phi(x,0) = -\frac{(0.+1.35057i)\left(1.e^{1.91x}-1.5\right)e^{(0.+0.95i)x}}{1.5+1.e^{1.91x}}, \tag{79}$$

and BCs as follows,

$$\Phi(0,t) = \frac{(0.+1.35057i)\left(1.e^{1.9t}-0.666667\right)e^{(0.+1.73868i)t}}{0.666667+1.e^{1.9t}}, \tag{80}$$

$$\Phi(1,t) = \frac{(0.+1.35057i)\left(1.e^{1.9t}-4.50206\right)e^{(0.+1.73868i)t+(0.+0.95i)}}{4.50206+1.e^{1.9t}}. \tag{81}$$

We construct the graphs of NFDS from Eq. (2) using the above IC and BCs and compare with the exact solution from the Eq. (45). So, Fig. 8 shows the graphical comparison of NSFD with exact solution $\Phi_{26}(x,t)$.

Example 9. The test problem is considered as follows,

$$i\Phi_t = -\frac{1}{2}\Phi_{xx} + V(x)\Phi + g|\Phi|^2\Phi + \sigma\dot{W}(t)\Phi, \tag{82}$$

using the initial condition as

$$\Phi(x,0) = \frac{(0.+0.777817i)\left(1.e^{1.1x}-0.666667\right)e^{(0.+1.95i)x}}{0.666667+1.e^{1.1x}}, \tag{83}$$

and BCs as follows,

$$\Phi(0,t) = -\frac{(0.+0.777817i)\left(1.e^{0.9t}-1.5\right)e^{(0.+3.43782i)t}}{1.5+1.e^{0.9t}}, \tag{84}$$

$$\Phi(1,t) = -\frac{(0.+0.777817i)\left(1.e^{0.9t}-4.50625\right)e^{(0.+3.43782i)t+(0.+1.95i)}}{4.50625+1.e^{0.9t}}. \tag{85}$$

We construct the graphs of NFDS from Eq. (2) using the above IC and BCs and compare them with the exact solution from the Eq. (48). So, Fig. 9 shows the graphical comparison of NSFD with exact solution $\Phi_{28}(x,t)$.

Results and discussion

In this study, the stochastic Gross–Pitaevskii equation (SGPE) is investigated analytically and numerically with multiplicative time noise. For the approximate solutions, the proposed stochastic NSFD scheme is constructed. The given numerical scheme is unconditionally stable and consistent with the given equation in the mean square sense. Meanwhile, for the sake of exact or analytical solutions, we choose two novel techniques namely, Sardar subequation (SSE) and modified exponential rational functional (MERF). So, solutions are successfully gained in the form of exponential, hyperbolic, and trigonometric forms. The results achieved are amazing and different from what has previously been published. Mainly, the comparison of graphical behavior of numerical solutions with some exact solutions that are extracted successfully drawn by using the initial and boundary conditions are given in the above section. Moreover, the Figs. 1–9 shows the wave structure or solitary wave solutions with the noise effect that appears in the literature for the sake of stochastic behavior. The SPGE model is applicable in the propagation of light in optical fiber, planar waveguides, and Bose–Einstein condensates confined to highly anisotropic sigar-shaped traps in the mean-field regime of dilute gases. The stochastc behavior is due to time noise and σ is the noisy strength which is a Boral function, These results are very useful for the physical appearance of the optical fibers and dilute gases. Mainly contribution is that the result shows a much similar behavior of numerical and exact solutions. So, our results will significantly contribute to the understanding of optical waves. The graphical structures of the earned solutions are successfully drawn under the suitable values of parameters that are given in Appendix "Graphics parameters". This unique work is successfully gained on Matlab 2015 and Mathematica 11.1 as well.

Conclusion

In this article, the stochastic Gross–Pitaevskii equation (SGPE) perturbed with multiplicative time noise in under investigation. The proposed stochastic non-standard finite difference (SNSFD) scheme is developed for the numerical solutions of the governing model. The stability of the scheme is proved by using the Von-Neumann criteria and the consistency is shown in the mean square sense. To seek exact solutions, we applied the Sardar subequation (SSE) and modified exponential rational functional (MERF) techniques. The exact solutions are constructed in the form of exponential, hyperbolic, and trigonometric forms. Additionally, we select the unique physical problem for the comparison of results. Finally, the comparison of the exact solutions with numerical solutions is drawn in the 3D and line plots for the different values of parameters.

CRediT authorship contribution statement

Muhammad Zafarullah Baber: Analysis. **Nauman Ahmed:** Analysis. **Muhammad Waqas Yasin:** Preparing figures. **Muhammad Sajid Iqbal:** Investigation. **Ali Akgül:** Supervision, Writing – editing. **Muhammad Bilal Riaz:** Supervision, Writing – editing. **Muhammad Rafiq:** Preparing figures. **Ali Raza:** Investigation.

Declaration of competing interest

The authors declare that they have no known competing financial interests or personal relationships that could have appeared to influence the work reported in this paper.

Data availability

No data was used for the research described in the article.

Appendix: Graphics parameters

The parameters that are used to drawn the Figs. 1–9 of some solutions are given below.

- For, Fig. 1 we use the parameters values as $\sigma = 0.3$, $n = 1000$, $N = 100$, $\alpha = 2.991$, $m = 1.91$, $l = 2.95$, $d = 0.01$, $g = 1$, $c = 0.09$, $p = 1$, $q = 2$ and $V(x) = 1$.
- For, Fig. 2 we use the parameters values as $\sigma = 0.3$, $n = 1000$, $N = 100$, $\alpha = 2.991$, $m = 2.91$, $l = 2.95$, $d = 0.01$, $g = 1$, $c = 0.9$, $p = 1$, $q = 2$ and $V(x) = 1$.
- For, Fig. 3 we use the parameters values as $\sigma = 0.3$, $n = 1000$, $N = 100$, $\alpha = 1.91$, $m = 1.9091$, $l = 0.905$, $d = 0.01$, $g = 1$, $c = 1.9$, and $V(x) = 1$.
- For, Fig. 4 we use the parameters values as $\sigma = 0.02$, $n = 100$, $N = 10$, $\alpha = 2.91$, $m = 0.9091$, $l = 2.5$, $d = 0.01$, $g = 1$, $c = 1.9$, and $V(x) = 1$.
- For, Fig. 5 we use the parameters values as $\sigma = 0.04$, $n = 1000$, $N = 100$, $\alpha = 0.991$, $\beta_1 = 3$, $\beta_0 = 0.9$, $l = 0.995$, $d = 0.3$, $g = 1$, $c = 0.9$, and $V(x) = 1$.
- For, Fig. 6 we use the parameters values as $\sigma = 0.04$, $n = 1000$, $N = 10$, $\alpha = 3.91$, $\beta_1 = 3.1$, $\alpha_1 = 1.1$, $l = 1.5$, $d = 0.01$, $g = 1$, $c = 1.9$, and $V(x) = 1$.
- For, Fig. 7 we use the parameters values as $\sigma = 0.01$, $n = 1000$, $N = 100$, $\alpha = 2.1$, $\beta_0 = 1.1$, $\alpha_0 = 0.2$, $l = 2.5$, $d = 0.01$, $g = 1$, $c = 3.9$, and $V(x) = 1$.
- For, Fig. 8 we use the parameters values as $\sigma = 0.04$, $n = 1000$, $N = 100$, $\alpha = 1.91$, $\beta_1 = 1.1$, $\alpha_1 = 1$, $l = 0.95$, $d = 0.01$, $g = 1$, $c = 1.9$, and $V(x) = 1$.
- For, Fig. 9 we use the parameters values as $\sigma = 0.1$, $n = 1000$, $N = 100$, $\alpha = 1.1$, $\beta_1 = 1$, $l = 1.95$, $d = 0.01$, $g = 1$, $c = 0.9$, and $V(x) = 1$.

References

[1] Carr LD, Leung MA, Reinhardt WP. Dynamics of the Bose–Einstein condensate: quasi-one-dimension and beyond. J Phys B: At Mol Opt Phys 2000;33(19):3983.
[2] Younis M, Seadawy AR, Baber MZ, Yasin MW, Rizvi ST, Iqbal MS. Abundant solitary wave structures of the higher dimensional sakovich dynamical model. Math Methods Appl Sci 2021.
[3] Sbitnev VI. Bohmian trajectories and the path integral paradigm: complexified Lagrangian mechanics. Int J Bifurcation Chaos 2009;19(07):2335–46.
[4] Whitham GB. Linear and nonlinear waves. New York: John Wiley & Sons, Inc.; 1974.
[5] Malomed BA, Stepanyants YA. The inverse problem for the Gross–Pitaevskii equation. Chaos 2010;20(1):013130.
[6] Kengne E, Vaillancourt R. Exact solutions of the Gross–Pitaevskii equation in periodic potential in the presence of external source. J Math Phys 2007;48(7):073520.
[7] Alfimov GL, Zezyulin DA. Nonlinear modes for the Gross–Pitaevskii equation—a demonstrative computation approach. Nonlinearity 2007;20(9):2075.
[8] Trallero-Giner C, Drake-Perez JC, López-Richard V, Birman JL. Formal analytical solutions for the Gross–Pitaevskii equation. Physica D 2008;237(18):2342–52.
[9] Bao W, Jaksch D, Markowich PA. Numerical solution of the Gross–Pitaevskii equation for Bose–Einstein condensation. J Comput Phys 2003;187(1):318–42.
[10] Tung SK. Probing an interacting bose gas in a quasi-two-dimensional trap (Doctoral dissertation), University of Colorado at Boulder; 2010.
[11] Ahn SM, Ha SY. Stochastic flocking dynamics of the Cucker–Smale model with multiplicative white noises. J Math Phys 2010;51(10):103301.
[12] Iqbal MS, Yasin MW, Ahmed N, Akgül A, Rafiq M, Raza A. Numerical simulations of nonlinear stochastic Newell–Whitehead–Segel equation and its measurable properties. J Comput Appl Math 2022;114618.
[13] Yasin MW, Iqbal MS, Ahmed N, Akgül A, Raza A, Rafiq M, Riaz MB. Numerical scheme and stability analysis of stochastic Fitzhugh–Nagumo model. Results Phys 2022;32:105023.
[14] Yasin MW, Iqbal MS, Seadawy AR, Baber MZ, Younis M, Rizvi ST. Numerical scheme and analytical solutions to the stochastic nonlinear advection diffusion dynamical model. Int J Nonlinear Sci Numer Simul 2021.
[15] Cheng K, Feng W, Gottlieb S, Wang C. A Fourier pseudospectral method for the good Boussinesq equation with second-order temporal accuracy. Numer Methods Partial Differential Equations 2015;31(1):202–24.
[16] Zhang C, Wang H, Huang J, Wang C, Yue X. A second order operator splitting numerical scheme for the good Boussinesq equation. Appl Numer Math 2017;119:179–93.
[17] Zhang C, Huang J, Wang C, Yue X. On the operator splitting and integral equation preconditioned deferred correction methods for the good Boussinesq equation. J Sci Comput 2018;75(2):687–712.
[18] Mirzaee F, Rezaei S, Samadyar N. Solution of time-fractional stochastic nonlinear sine-Gordon equation via finite difference and meshfree techniques. Math Methods Appl Sci 2021.
[19] Mirzaee F, Rezaei S, Samadyar N. Application of combination schemes based on radial basis functions and finite difference to solve stochastic coupled nonlinear time fractional sine-Gordon equations. Comput Appl Math 2022;41(1):1–16.
[20] Mirzaee F, Rezaei S, Samadyar N. Solving one-dimensional nonlinear stochastic Sine–Gordon equation with a new meshfree technique. Int J Numer Modelling, Electron Netw Devices Fields 2021;34(4):e2856.
[21] Mirzaee F, Rezaei S, Samadyar N. Numerical solution of two-dimensional stochastic time-fractional Sine–Gordon equation on non-rectangular domains using finite difference and meshfree methods. Eng Anal Bound Elem 2021;127:53–63.
[22] Mirzaee F, Sayevand K, Rezaei S, Samadyar N. Finite difference and spline approximation for solving fractional stochastic advection-diffusion equation. Iran J Sci Technol Trans A Sci 2021;45(2):607–17.
[23] Mirzaee F, Samadyar N. Implicit meshless method to solve 2D fractional stochastic tricomi-type equation defined on irregular domain occurring in fractal transonic flow. Numer Methods Partial Differential Equations 2021;37(2):1781–99.
[24] Samadyar N, Ordokhani Y, Mirzaee F. Hybrid taylor and block-pulse functions operational matrix algorithm and its application to obtain the approximate solution of stochastic evolution equation driven by fractional Brownian motion. Commun Nonlinear Sci Numer Simul 2020;90:105346.
[25] Mirzaee F, Samadyar N. Combination of finite difference method and meshless method based on radial basis functions to solve fractional stochastic advection–diffusion equations. Eng Comput 2020;36(4):1673–86.
[26] Samadyar N, Ordokhani Y, Mirzaee F. The couple of Hermite-based approach and Crank–Nicolson scheme to approximate the solution of two dimensional stochastic diffusion-wave equation of fractional order. Eng Anal Bound Elem 2020;118:285–94.
[27] Mirzaee F, Samadyar N. Numerical solution of time fractional stochastic Korteweg–de Vries equation via implicit meshless approach. Iran J Sci Technol Trans A Sci 2019;43(6):2905–12.
[28] Ghany HA, Hyder AA, Zakarya M. Exact solutions of stochastic fractional Korteweg de–Vries equation with conformable derivatives. Chin Phys B 2020;29(3):030203.
[29] Mohammed WW, Ahmad H, Boulares H, Khelifi F, El-Morshedy M. Exact solutions of Hirota–Maccari system forced by multiplicative noise in the Itô sense. J Low Freq Noise Vib Act Control 2022;41(1):74–84.
[30] Tari H, Ganji DD, Babazadeh H. The application of He's variational iteration method to nonlinear equations arising in heat transfer. Phys Lett A 2007;363(3):213–7.
[31] Assas LM. Approximate solutions for the generalized KdV–Burgers' equation by He's variational iteration method. Phys Scr 2007;76(2):161.
[32] Rani M, Bhatti HS, Singh V. Exact solitary wave solution for higher order nonlinear schrodinger equation using He's variational iteration method. Opt Eng 2017;56(11):116103.
[33] Nisar KS, Alsallami SAM, Iqbal MS, Baber MZ, Tarar MA. On the exact solutions of nonlinear extended Fisher-Kolmogorov equation by using the He's variational approach. AIMS Math. 2022;7(8):13874–86.
[34] Soliman AA, Abdo HA. New exact solutions of nonlinear variants of the RLW, the PHI-four and Boussinesq equations based on modified extended direct algebraic method. 2012, arXiv preprint arXiv:1207.5127.
[35] Rehman HU, Seadawy AR, Younis M, Rizvi STR, Anwar I, Baber MZ, Althobaiti A. Weakly nonlinear electron-acoustic waves in the fluid ions propagated via a (3+1)-dimensional generalized Korteweg–de-Vries–Zakharov–Kuznetsov equation in plasma physics. Results Phys 2022;33:105069.
[36] Zayed EM, Gepreel KA. Some applications of the G' G-expansion method to non-linear partial differential equations. Appl Math Comput 2009;212(1):1–13.
[37] Younis M, Seadawy AR, Baber MZ, Husain S, Iqbal MS, Rizvi STR, Baleanu D. Analytical optical soliton solutions of the Schrödinger-Poisson dynamical system. Results Phys 2021;27:104369.
[38] Zayed EM, Al-Nowehy AG. The ϕ^6-model expansion method for solving the nonlinear conformable time-fractional Schrödinger equation with fourth-order dispersion and parabolic law nonlinearity. Opt Quantum Electron 2018;50(3):1–19.
[39] Bilal M, Ahmad J. Investigation of optical solitons and modulation instability analysis to the Kundu–Mukherjee–Naskar model. Opt Quantum Electron 2021;53(6):1–22.
[40] Nakamura A. Surface impurity localized diode vibration of the Toda lattice: Perturbation theory based on Hirota's bilinear transformation method. Progr Theoret Phys 1979;61(2):427–42.
[41] Younas U, Ren J, Baber MZ, Yasin MW, Shahzad T. Ion-acoustic wave structures in the fluid ions modeled by higher dimensional generalized Korteweg–de Vries–Zakharov–Kuznetsov equation. J Ocean Eng Sci 2022.
[42] Ahmed N, Bibi S, Khan U, Mohyud-Din ST. A new modification in the exponential rational function method for nonlinear fractional differential equations. Eur Phys J Plus 2018;133(2):1–11.
[43] Aksoy E, Kaplan M, Bekir A. Exponential rational function method for space–time fractional differential equations. Waves Random Complex Media 2016;26(2):142–51.
[44] Rahaman H, Hasan MK, Ali A, Alam MS. Implicit methods for numerical solution of singular initial value problems. Appl Math Nonlinear Sci 2021;6(1):1–8.
[45] Liu D, He W. Numerical simulation analysis mathematics of fluid mechanics for semiconductor circuit breaker. Appl Math Nonlinear Sci 2021.
[46] Veeresha P, Ilhan E, Prakasha DG, Baskonus HM, Gao W. Regarding on the fractional mathematical model of Tumour invasion and metastasis. CMES Comput Model Eng Sci 2021;127(3):1013–36.
[47] Delgado MF, Esenarro D, Regalado FFJ, Reátegui MD. Methodology based on the NIST cybersecurity framework as a proposal for cybersecurity management in government organizations. 3 c TIC: cuadernos de desarrollo aplicados a las TIC. 2021;10(2):123-41.
[48] Wang Y. Application of numerical method of functional differential equations in fair value of financial accounting. Appl Math Nonlinear Sci 2022;7(1):533–40.
[49] Xu L, Aouad M. Application of Lane-Emden differential equation numerical method in fair value analysis of financial accounting. Appl Math Nonlinear Sci 2021.
[50] Yadav AKS, Sora M. An optimized deep neural network-based financial statement fraud detection in text mining. 3c Empresa: investigación y pensamiento crítico. 2021;10(4):77-105.
[51] Rogel-Salazar J. The Gross–Pitaevskii equation and Bose–Einstein condensates. Eur J Phys 2013;34(2):247.
[52] Kamrani M, Hosseini SM. The role of coefficients of a general SPDE on the stability and convergence of a finite difference method. J Comput Appl Math 2010;234(5):1426–34.
[53] Iqbal MS, Seadawy AR, Baber MZ. Demonstration of unique problems from soliton solutions to nonlinear Selkov–Schnakenberg system. Chaos Solitons Fractals 2022;162:112485.
[54] Seadawy AR, Younis M, Iqbal MS, Baber MZ, Rizvi ST, Raheem A. Soliton behavior of algae growth dynamics leading to the variation in nutrients concentration. J King Saud Univ-Sci 2022;34(5):102071.
[55] Akinyemi L, Akpan U, Veeresha P, Rezazadeh H, Inc M. Computational techniques to study the dynamics of generalized unstable nonlinear Schrödinger equation. J Ocean Eng Sci 2022.
[56] Seadawy AR, Rizvi ST, Mustafa B, Ali K, Althubiti S. Chirped periodic waves for an cubic-quintic nonlinear Schrödinger equation with self steepening and higher order nonlinearities. Chaos Solitons Fractals 2022;156:111804.

[57] Hussain R, Imtiaz A, Rasool T, Rezazadeh H, Inc M. Novel exact and solitary solutions of conformable Klein–Gordon equation via Sardar-subequation method. J Ocean Eng Sci 2022.
[58] Cinar M, Secer A, Ozisik M, Bayram M. Derivation of optical solitons of dimensionless Fokas–Lenells equation with perturbation term using Sardar sub-equation method. Opt Quantum Electron 2022;54(7):1–13.
[59] Asjad MI, Munawar N, Muhammad T, Hamoud AA, Emadifar H, Hamasalh ... FK, Khademi M. Traveling wave solutions to the Boussinesq equation via Sardar sub-equation technique. AIMS Math 2022;7(6):11134–49.
[60] Bilal M, Younis M, Ahmad J, Younas U. Investigation of new solitons and other solutions to the modified nonlinear Schrödinger equation in ocean engineering. J Ocean Eng Sci 2022.
[61] Sarwar A, Gang T, Arshad M, Ahmed I, Ahmad MO. Abundant solitary wave solutions for space–time fractional unstable nonlinear Schrödinger equations and their applications. Ain Shams Eng J 2022;101839.
[62] Li Y, Lu D, Arshad M, Xu X. New exact traveling wave solutions of the unstable nonlinear Schrödinger equations and their applications. Optik 2021;226:165386.
[63] Althobaiti A, Althobaiti S, El-Rashidy K, Seadawy AR. Exact solutions for the nonlinear extended KdV equation in a stratified shear flow using modified exponential rational method. Results Phys 2021;29:104723.